INTERNATIONAL JOURNAL FOR NUMERICAL METHODS IN FLUIDS
Int. J. Numer. Meth. Fluids 2000; **32**: 711–724

Numerical prediction of flow in a model of a (potential) soft acting peristaltic blood pump

S. Natarajan and M. R. Mokhtarzadeh-Dehghan*

Department of Mechanical Engineering, Brunel University, Uxbridge, Middlesex UB8 3PH, U.K.

SUMMARY

This paper presents a numerical study of the flow field in a novel 'soft' acting peristaltic pump. The pump has potential applications wherever pumping of biological or sensitive fluids with reduced damage is required. The application of the device presented is as a blood pump. The model of the pump comprises a cylindrical tube that forms three chambers. The walls of these chambers move radially as a function of time. The pumping action is initiated by applying phased movement between the chambers. The flow is treated as laminar, unsteady, incompressible, Newtonian, and with a moving boundary. The governing equations are solved using a finite element method (FEM). An operating speed of 60 cycle $\min^{-1}$ has been chosen. The results show that a periodic solution can be achieved after four cycles. The velocity field, streamline and shear stress are presented and discussed. The flow has generally a two-way pulsatile nature, moving forwards and backwards. However, at the outlet, there is a net outflow over one cycle against a zero pressure head. Net flow linearly decreases to zero with increasing pressure head. Copyright © 2000 John Wiley & Sons, Ltd.

KEY WORDS: blood; computational fluid dynamics; finite element; moving boundary; numerical; peristaltic; pump

1. INTRODUCTION

A major difficulty in the design of blood pumping systems is in avoiding cellular damage. A common way to meet this requirement is to use rotary peristaltic pumps. These pumps force the fluid to move by the action of rollers over the tube. However, the tubes are often forced shut, where they may still cause damage because of high contact forces and high localized viscous shears. Therefore, improved pumping systems are still needed. The potential range of applications for a new pump is large, especially where particulate living matter is to be pumped, e.g. in the brewing and biochemical industries, for serum and vaccine production, for dialysis and for blood pumps. Blood pumps are needed particularly during heart bypass surgery, where it is required to stop the heart.

* Correspondence to: Department of Mechanical Engineering, Brunel University, Uxbridge, Middlesex UB8 3PH, U.K.

Received May 1998
Revised August 1998

Rotary peristaltic pumps are widely used for blood pumping applications because they fulfil the majority of the blood pumping requirements. There have been a number of theoretical studies on peristaltic pumping, however, these involve sinusoidal, infinitely long, two-dimensional, continuous peristaltic waves [1–3]. Fung and Yih [1] were among the first to study the fluid mechanics of small amplitude peristaltic waves. Shapiro *et al.* [2] studied small amplitude, slow moving Newtonian flows and identified unique features of peristaltic flows, such as 'reflux' and 'trapping' in the context of biological vessels. Reflux is a feature where the mean retrograde velocity of the fluid is opposite to the direction of wave propagation. Trapping occurs where there is a stationary recirculation and fluid is unable to move with the main flow stream. Provost and Schwarz [3] presented solutions for long wavelengths and large amplitudes. They also predicted the possibility of mean axial flow that opposes the direction of wave propagation. Aspects of this type of flow are also seen in the discrete pumping model of the present study. There is a lack of theoretical work applied to the potential of discrete (discontinuous) peristaltic pumping. Actual rotary peristaltic pumps used for blood pumping applications cause a complex three-dimensional curved deformation of the tube over a finite length. Li and Brasseur [4] studied flow in finite length tubes with continuous waves and found that the pumping performance depends on the number of waves, the phase of the first and last waves, and the degree of tube occlusion. In addition, this theoretical work shows that peristalsis produces very large shear stresses in the region of maximal occlusion. These characteristics have important consequences for fluids like blood, particularly in the activation of blood to form a thrombus.

There have been a few studies on predicting damage to red blood cells (haemolysis). It is well known that viscous shear stresses and Reynolds stresses are a major cause of blood trauma [5,6]. Blackshear and Blackshear [5] among many others have shown the need to consider the magnitude and time history of these parameters to estimate mechanical trauma and platelet activation. Bludszuweit [6] used these findings to produce a general theoretical blood damage prediction model based on the mechanical loading and damage accumulation. The work was applied to centrifugal pumps, but concludes that accurate prediction requires the detailed study of frequency and amplitude of stress loading on blood elements.

In practice it is extremely difficult to obtain detailed loading and history on blood components, yet this information is needed and numerical techniques, such as computational fluid dynamics (CFD), have recently provided a possible way of determining these conditions. Some CFD models have been applied to predict flow conditions past a fixed stenosis [7,8]. Tu *et al.* [7] studied steady and pulsating flow through a range of rigid stenosis and found that the unsteady flow past a stenosis produces features not seen in steady flow alone. More recently, Bluestein *et al.* [8] simulated a range of steady state flow conditions through a stenosis and was able to correlate experimental observations of platelet deposition with predicted regions of high wall shear stress. Some transient artificial heart valve flows and wall-driven heart chamber flows have been predicted and compared with experimental data. These have shown that CFD techniques can qualitatively predict complex observed features of interest to the physiologist. However, due to the difficulty in modelling the complex physical and chemical properties of blood, care must be taken on the quantitative results since they generally do not agree as well.

2. THE PHYSICAL PUMP

In studying a potentially new discrete peristaltic blood pump, it is suggested that the synchronized motions of the walls of a section of tube containing the fluid can achieve net pumping of the fluid. For example, a single straight tube, divided into three sections, can be made pump a fluid if the motions of the walls of each section are synchronized in a pre-defined manner. The overall aim of the present work is to examine this principle theoretically and assess the potential of such a peristaltic pump. Finite element analysis of the fluid flow in a tube with moving boundaries can be used to gain a better understanding of the fluid flow behaviour within the pump. This is considered to be an important step towards the improvement of the design.

Figure 1 shows a schematic representation of a prototype peristaltic pump. This pump works by a principle of occlusion and displacement. It is made up of a single silicone tube surrounded by three pumping chambers. Each chamber is isolated from its neighbours making it possible to vary the outer pressure on the silicone tube in each compartment. The pressure difference between the inside and the outside of the tube distorts the silicone tubing, such that it squeezes the fluid inside the tube. When the pressurizing cycles in the three chambers are synchronized the pump is capable of average peristaltic pumping of the fluid, in one direction, inside the tube. Note that the motion of this pump is significantly different from the continuous peristaltic wave motion noted before.

3. THE FINITE ELEMENT MODEL

The finite element model is based on the prototype pump, consisting of three chambers and has the same overall dimensions. While the boundaries of the three chambers are made to move independently, the tube wall is fixed at intermediate positions. Therefore, at one instant in time, the computational domain may take the shape shown in Figure 2. Two fixed shorter sections are located between chambers 1 and 2, and between chambers 2 and 3. The position of the tube wall for one chamber at different times during the cycle is shown in Figure 3. The dimensions based on the prototype pump are $D = 6.0 \times 10^{-3}$ m, $L = 50 \times 10^{-3}$ m,

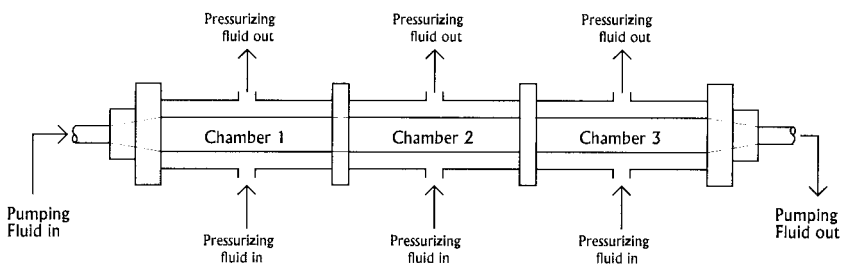

Figure 1. Schematic of 'soft' acting peristaltic pump.

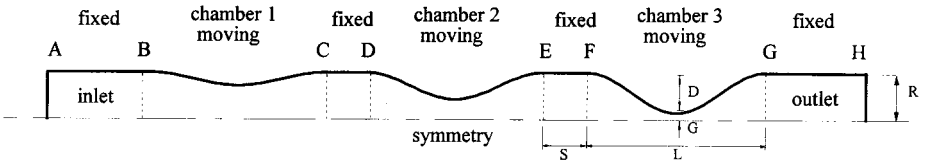

Figure 2. Typical geometry at one instant during the pumping cycle.

$G = 0.5 \times 10^{-3}$ m, $S = 30 \times 10^{-3}$ m, and $R = 6.5 \times 10^{-3}$ m. Figure 2 shows two additional chambers with fixed walls at each end. These were added to increase computational stability only and will be referred to later.

The position of every point on the moving boundary is defined by radial displacement r relative to the undistorted position of the tube. The distance r can be obtained from a defined function. Two functions were considered in the following form in order to produce the deflection shown in Figure 3(a) and (b). The displacement functions (1) and (2) vary with time t and longitudinal displacement z in the form

$$r = Cz^2(z-L)^2\left[\frac{1}{2} - \frac{1}{2}\cos 2\pi t\right] \tag{1}$$

$$r = Cz^2(z-L)^2[\sin 2\pi t] \tag{2}$$

where C and L are constants and the term in square brackets represents a time function that oscillates sinusoidally with time t. In Equation (1), the time function varies between 0 and $+1$, whereas in Equation (2) it varies between -1 and $+1$. The boundary conditions for Equations (1) and (2) are given in Table I. The value of constant C can be found by substituting the time at maximum deflection into Equation (1) or (2) giving

$$C = -\frac{16D}{L^4} \tag{3}$$

The pump works at a frequency of 1 cycle s^{-1}. Each of the three chambers is run out of phase with its neighbour by introducing a time lag ϕ. A time lag of $\frac{1}{3}$ s is chosen so that the motion is smooth and continuous over one pump cycle. The timing sequence is such that constriction occurs in the sequence chamber 1 followed by chamber 2, and then chamber 3. This is the usual sequence for continuous peristaltic pumping.

When a cylindrical section of a flexible tube collapses, it behaves in a complex manner. Here, however, it is assumed that the cross-section remains circular at all times. Hence, the model maintains its axisymmetric shape. There is, therefore, no tangential velocity (swirl) component $\mathbf{V}_\theta$. No-slip condition was applied to all tube walls. As a result, at the wall the fluid has the same radial velocity as the wall. The radial velocity of the tube wall can be obtained from differentiation of Equations (1) and (2) with respect to time.

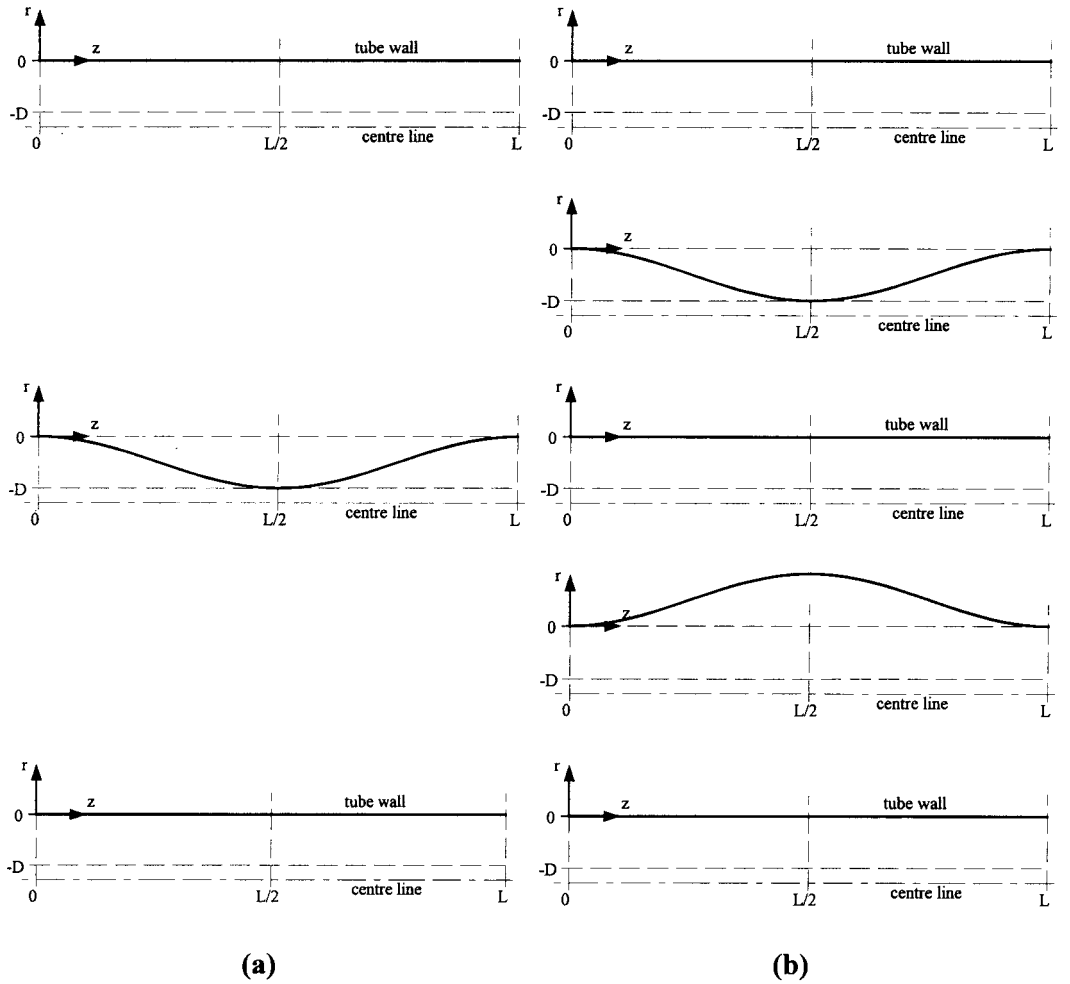

Figure 3. Position of first chamber wall at different time intervals shown in Table I. (a) Equation (1); (b) Equation (2).

The radial velocity on the symmetry line was set to zero. At the inlet and outlet, the axial velocity was free, but the radial velocity was set to zero. The fluid elements at all other positions were free to consist of axial and radial velocity components. Initially, there was no pressure gradient applied to the flow. This not only simplifies the problem but also allows the effects of the moving boundary alone to be investigated. The fluid was assumed to be Newtonian, homogenous, incompressible and isothermal. Also, the fluid was at rest at $t = 0.0$ s, hence any subsequent motion is determined by the motion of the boundaries alone.

Table I. Boundary conditions for the displacement functions.

t (s)	Equation (1)	Equation (2)
0.00	$r=0;\ 0\le z\le L$	$r=0;\ 0\le z\le L$
0.25		$r=-D;\ z=L/2$
0.50	$r=-D;\ z=L/2$	$r=0;\ 0\le z\le L$
0.75		$r=+D;\ z=L/2$
1.00	$r=0;\ 0\le z\le L$	$r=0;\ 0\le z\le L$

For simplicity, the fluid properties of water at 20°C were used. The flow was assumed to be laminar.

The parameters upon which the performance of the pump depends are: number of coupled chambers, time function, phase difference between chambers, shape of the deforming wall, physical dimensions of pump, applied forces (variable operating pressure gradient or body forces) and fluid properties. The model described here is based around the simplest aspects of the above variables. It was chosen deliberately to study the effect of discrete peristaltic pumping in a simple set-up.

4. COMPUTATIONAL DETAILS

The governing equations were the two components of the momentum equation, in radial and axial directions, and the continuity equation. They were solved using an axisymmetric two-dimensional grid containing 2600 quadrilateral four-node elements. This low-order scheme was initially chosen to keep the overall size of the problem manageable owing to the large number of required time steps. Later it will be shown that this solution is grid-independent. The deformation of the grid varied according to the boundary condition function described in Equations (1) and (2). A section of this deforming grid is shown in Figure 4. A fully coupled Newton–Raphson solution algorithm was employed. The pressure was derived using the penalty function method. The initial condition was obtained from the linear Stokes flow solution.

The solution was said to have converged when two criteria were satisfied. First, the sum of residuals for all cells normalized with respect to a reference value fell below 10^{-5}. Second, the change in velocity for all cells as a fraction of current velocity also fell below 10^{-5}. This was usually achieved after ten iterations at each time step. The magnitude of each time step was variable and determined by the local truncation error. Figure 5 shows the time step varying between 0.0004 s and 0.02 s. The time integration method was backward Euler.

Since the nature of the pump is periodic, the solution was allowed to continue for a number of cycles until a repeatable flow field was achieved and the effect of initial conditions was minimized. Four cycles, consisting of 1225 time steps, were required to achieve this condition. The computation time was 5 processor hours on a Sun Sparc Station 20.

The flow experiences significant changes throughout the pumping sections, so it was found necessary to separate the inlet and outlet ends of the computational domain away from the

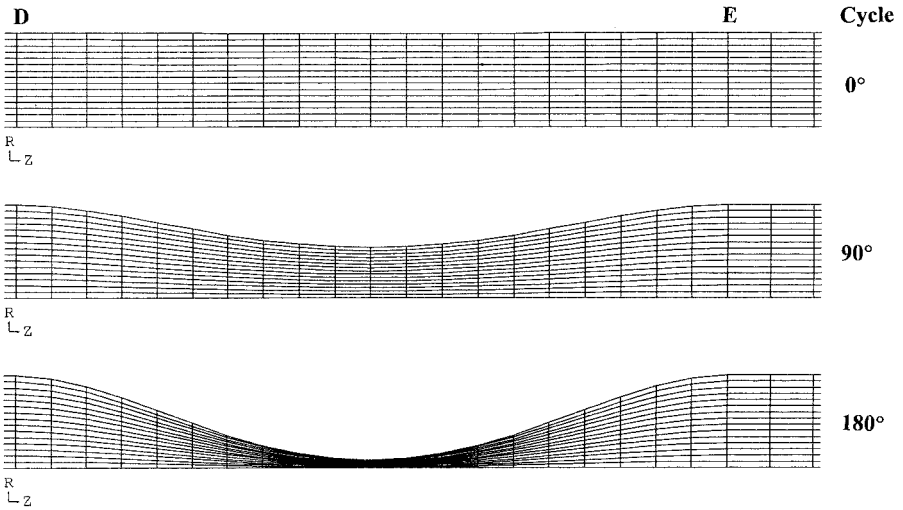

Figure 4. Nature of the deforming grid at extreme and intermediate stages of the pumping cycle 0°, 90°, 180°.

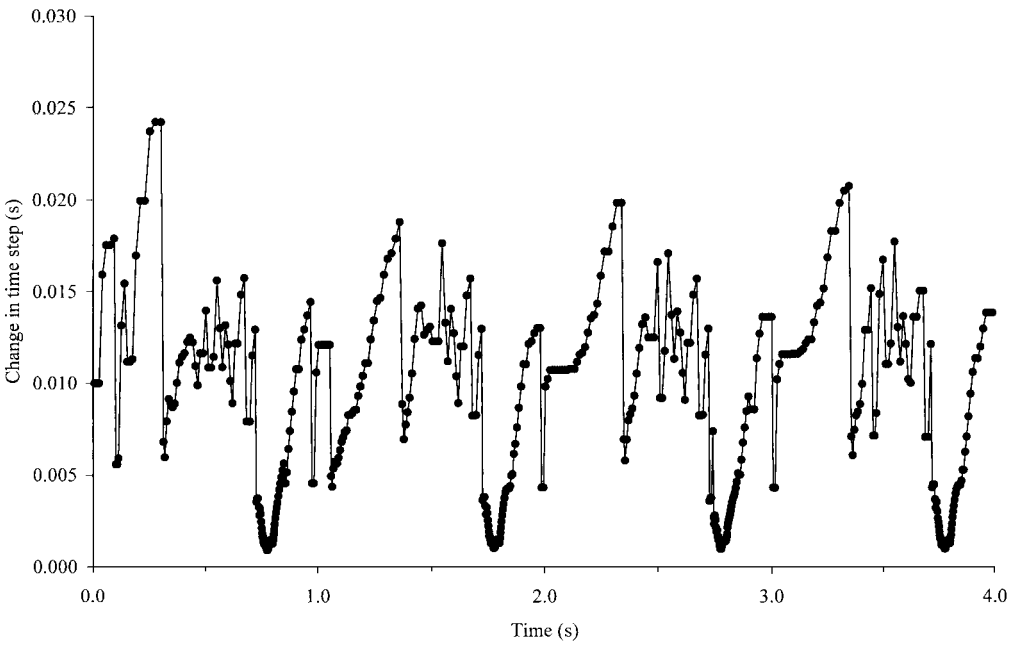

Figure 5. Change in time step over four cycles.

three main chambers, as shown in Figure 2. The walls of these sections were fixed. There was no special treatment at the ends other than defining zero radial velocity, which helped convergence and stability of the solution.

The finite element program FIDAP v7.51 [9] was used to solve the equations and implement the above boundary and initial conditions.

5. RESULTS

The results are mainly presented for the displacement function given in Equation (1) for zero pressure head. Figure 6 shows the time history of the velocity profile at the exit, during four cycles, from the start of solution at $t = 0.0$ s to the end of solution at $t = 4.0$ s. The improved repeatability of the solution as time progresses can be seen. The last two cycles (2–4 s) are significantly more similar than the first two cycles (0–2 s). The change in net volume flow rate at the outlet between the last two cycles was less than 0.5%. The velocity history at the exit suggests that it has reached periodic repeatability.

Plate 1(a) and (b) shows the inlet and outlet velocity vector fields during the last cycle at every 0.2 s interval. Plate 2(a) and (b) shows the equivalent streamline contours of the vector field. The axial velocity profiles at the end of chamber 3 and at different times during the fourth cycle are shown in Figure 7. Integration of the velocity profile yields the instantaneous volume flow rate for both displacement functions shown in Figure 8.

Figure 9 shows the net flow rate with various pressure heads for both displacement functions. The Reynolds number and Womersley number based on a typical flow velocity of 0.1 m s^{-1} and frequency of 1 Hz in a non-constricted section is 1300 and 16.3 respectively.

To study the effect of different types of elements on the flow rate, solutions where also obtained for 5828 four-node elements and 3290 nine-node elements. The results showed,

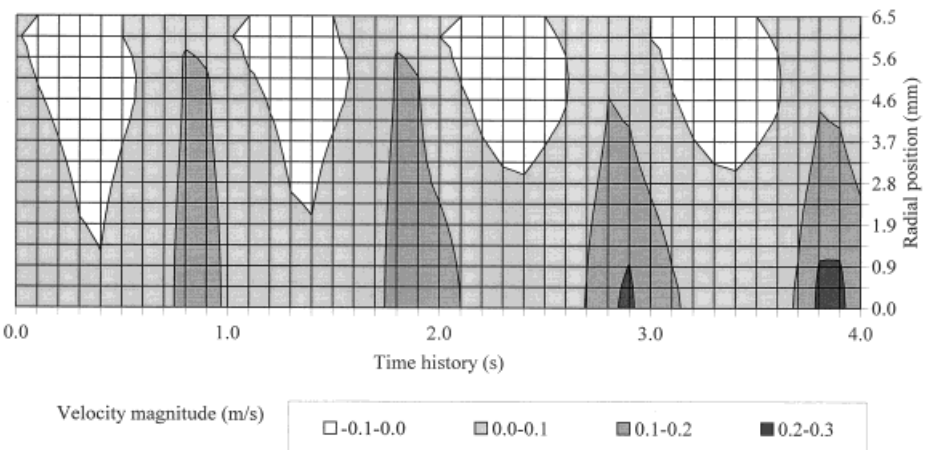

Figure 6. Repeatability of velocity magnitude at section H (exit) over four cycles.

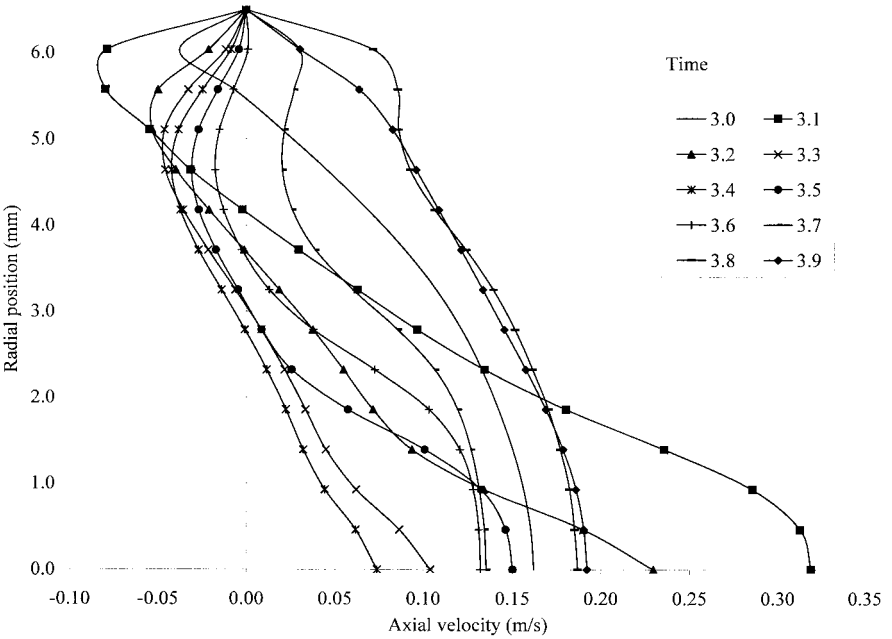

Figure 7. Velocity profiles at the end of chamber 3 section G.

compared with the 2600 four-node elements, a 1.2% and 0.7% difference in volume flow rate respectively. In addition, both these simulations contained elements with approximately half the aspect ratio of the first, indicating that these solutions produce gross results independent of the grid.

6. DISCUSSION

Velocity fields show that the contracting and expanding nature of the three chambers causes the fluid to behave differently than if only a single chamber was involved. The flow predicted in each chamber was similar to that obtained by the analytical solution of flow in an expanding or contracting pipe, as described by Uchida and Aoki [10]. The influence of the curved boundary and the effect of multiple chambers were to distort the direction of net flow in or out of a chamber.

Plates 1 and 2 ($t = 3.0$ s) show the fluid accelerating through the narrowing and recirculating immediately downstream of chamber 3. The velocity profile at a radial section through G at $t = 3.0$ s (Figure 7) shows that the flow is mainly in the positive direction. Soon after this, at $t = 3.1$ s, the brief appearance of a central jet can be seen in Figure 7 causing a peak in the velocity profile together with reversing flow near the walls.

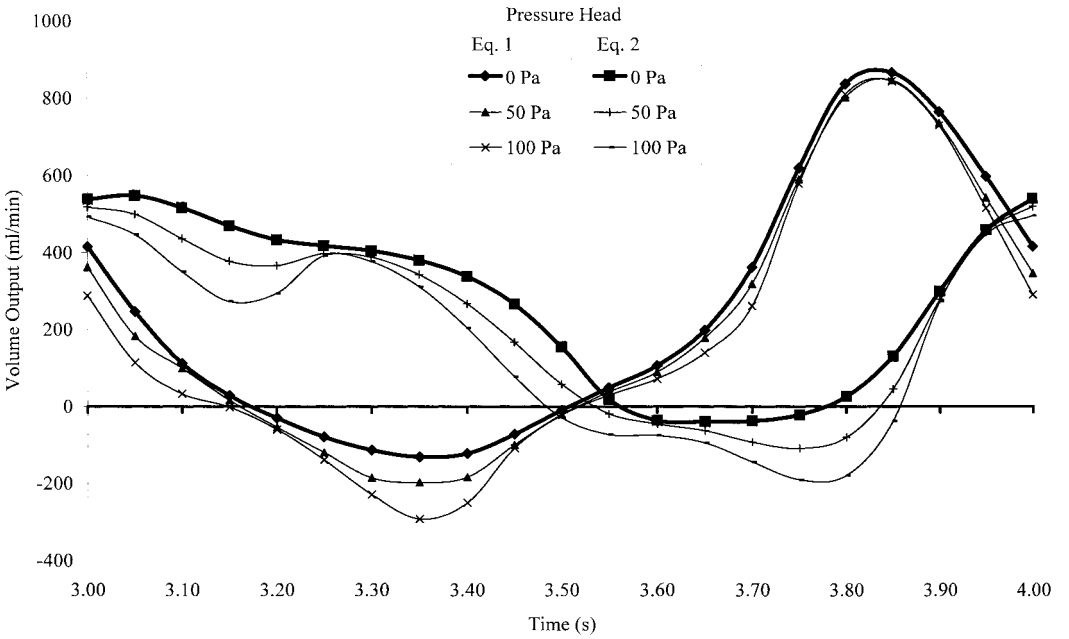

Figure 8. Volume output against time over one cycle for various pressure heads.

At $t = 3.2$ s, the recirculation region occupies a significant portion of the outlet duct. Due to the viscous nature of the flow, the flow in fact never reattaches within the computational domain and there is a partial reversal of flow at the outlet, compare $t = 3.0$ s and $t = 3.2$ s (Plate 1(b)). During this time the net outflow rapidly decreases to zero, as shown in Figure 8. At the same time the higher velocity of the jet causes it to shear past the surrounding slower fluid and move downstream (Plate 1(b)). The axial jet causes the surrounding annular fluid to decelerate, reverse and recirculate as a result of the low-pressure region created behind the displacing jet. The effect is to rapidly accelerate the surrounding fluid in the opposite direction to the jet pulse, hence creating a mixing and dissipating annular vortex.

As the pulse jet slows and weakens in intensity, the reverse flow is maintained by the low pressure as a result of the currently expanding wall of chamber 3. Figure 8 shows that the reverse net outflow begins at $t = 3.2$ s. Figure 8 also shows the pump reaches its maximum reverse flow rate of 130 ml min^{-1} at $t = 3.35$ s. By $t = 3.6$ s, the jet pulse is very weak and elongated and the back flow is rapidly decelerating because the chamber has fully expanded. By $t = 3.8$ s, the contracting cycle begins. As the chamber contracts, reducing in volume, the flow can only move forward because chamber 2 is effectively closed at this time. It is between 3.8 and 3.9 s that the pump reaches its maximum forward flow rate of 870 ml min^{-1}.

Figure 8 shows that over the whole cycle the forward flow exceeds the reverse, and produces a net forward output of 230 ml min^{-1}. This indicates that the first displacement function (Equation (1)) is suitable for net pumping. However, we have seen that even with this

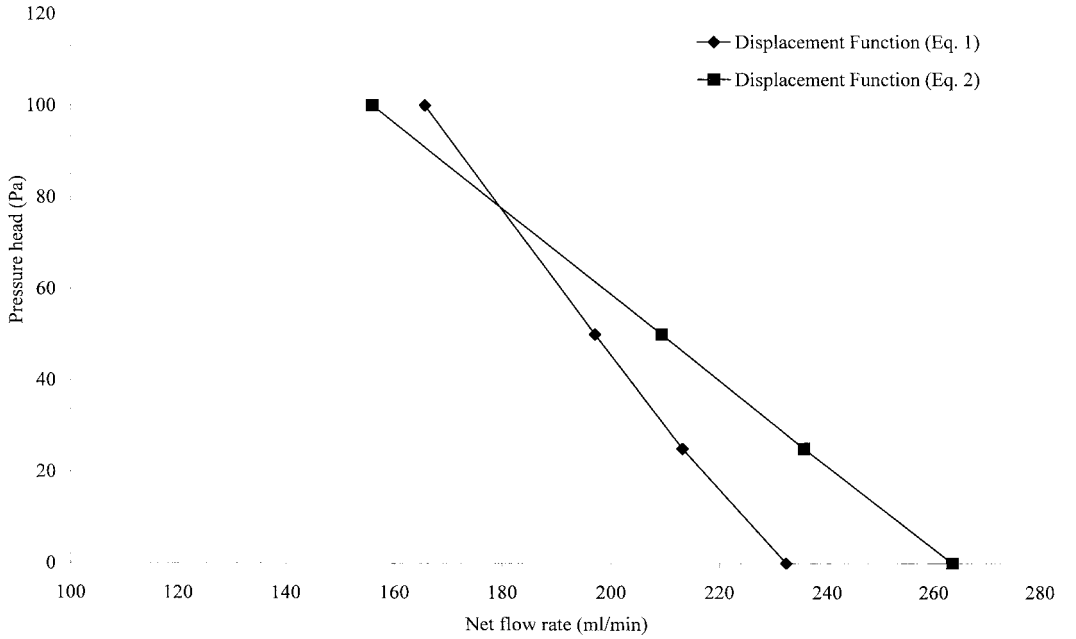

Figure 9. Pressure head against net flow rate.

non-optimized configuration relatively large flow rates are seen during the cycle, so an increased potential pumping ability exists. Figure 8 also shows that the results from the second displacement function (Equation (2)) describe a completely different flow characteristic. This flow profile produces a forward flow rate of 260 ml min^{-1}. This shows that with the correct selection of displacement function it may be possible to produce the required mean flow rate and flow profile.

Figure 9 shows the effect of a pressure gradient on the mean net flow. Both displacement functions show a decreasing net flow rate at the outlet with increasing pressure head. For the four pressure heads considered, the relationship is approximately linear. In addition the lower gradient of the second displacement function indicates that this pumping characteristic is more influenced by changes in pressure gradient. This influence is also seen by the spread of curves in Figure 8 for Equation (2).

The magnitude and duration of shear experienced by blood components in the pump are important factors affecting its performance. High shear causes cellular components to spin violently and rupture their membranes. These components, particularly platelets, may respond to this type of flow by triggering a clotting response. Activating platelets in this manner should be kept a minimum. In the present study, it is possible to predict regions within the flow field and the instants of time, or time periods, within which high shear levels occur. The regions of maximum shear rate have been found to occur when the chambers are approaching the maximum stenosed position. This agrees in principle with the findings of Robertson *et al.* [11],

who also predicted maximum shear stress at the throat of a transversely moving boundary. The maximum instantaneous shear rate is estimated to be $10^4\,s^{-1}$ occurring at $t = 3.1$ s between section G and H for a maximum of 0.1 s (Plates 1 and 2). This gives an approximate maximum product of particle shear rate $\times$ resident time (duration) of 10^3.

Currently, there is little quantitative evidence to suggest how flow mechanics initiate platelet activation. The magnitudes and duration of various flow conditions responsible for platelet activation can only be determined through experimental investigations using actual blood. Ramstack *et al.* [12] observed experimentally that a shear–duration product of 10^3 was necessary to activate platelets under constant shear rates. More recently, Bluestein *et al.* [8] showed that platelets become activated when passing through a stenosis in a closed loop circuit. The estimated maximum shear–duration product was 500. This is half the maximum value present in the current device and clearly indicates that design improvement and optimization is required to improve the potential of this pumping method.

The prediction by this laminar model is a rapid mixing nature of the flow and a strong tendency for the transversely moving boundary to form momentary jets. These provide the initial momentum to form vortices that continue to move the whole structure forward. The energy within the vortex is dissipated as it shears past the surrounding fluid and decreases in speed. In reality, large accelerations and decelerations seen may result in outbursts of turbulence. Both simulations and experiments accounting for momentary turbulence will be necessary to study the way in which these vortices rapidly form, interact with reversing flow, and dissipate.

The dynamic velocity fields produced show a unique intrinsic pulsatile and agitating ability of the pump. However, it is uncertain at this stage how suitable this type of flow is for blood pumping applications. The advantages and disadvantages of pumping a live medium such as blood depend on the exact nature of the flow and the behaviour of its components. Particle paths need to be modelled to calculate the acceleration, shear history and duration of the related forces on typical and extreme trajectories. There also is a need to account for the non-Newtonian properties of blood. These become important particularly at low shear rates. It has been seen that the flow oscillates resulting in many temporary regions of stationary or slow shearing fluid.

Only with further study will it be possible to harness the unique characteristics of a pump such as this. This may lead to alternative pumping applications. The simulation of the real flow presents more of a challenge, since it contains compliant moving walls with the potential benefits of gaseous diffusion across the walls (cardio-pulmonary applications) and localized momentary turbulence.

7. CONCLUSION

The simple discrete peristaltic pumping method described produces complex flow conditions purely due to the movement of its boundaries. The features predicted are regions of recirculation, jets and vortices in a constant state of flux. When using a small displacement function (Equation (1)), the net flow for a zero pressure gradient was $230\,ml\,min^{-1}$ in the direction of the peristaltic wave (for the model studied). However, a larger displacement

the peristaltic wave (for the model studied). However, a larger displacement function (Equation (2)) produced a net forward flow of 260 ml min^{-1} for zero pressure head. Both these net flows decrease linearly with increasing opposing pressure gradient up to at least 100 Pa. Shear rates were found to be highest for the short period when the jets formed.

This is a first step towards attempting to predict and understand the flow in a relatively new pump. This discrete peristaltic pumping mechanism provides a possible alternative to the continuous rotary peristaltic pumps. With further study, appropriate design improvements can achieve superior fluid dynamic performance to existing biological pumps.

ACKNOWLEDGMENTS

The authors acknowledge the suggestion and continued interest of this work from Tony Anson, Anson Medical Ltd.

APPENDIX A. NOMENCLATURE

C	physical constant
D	maximum radial displacement of chamber $= R - G$
G	minimum radius at maximum wall deflection
L	axial length of one moving boundary chamber
r	radial displacement
R	undistorted radius of the tube
S	length of intermediate spaces between chambers
t	time
$\mathbf{V}$	velocity vector
z	longitudinal position

Greek letters

ϕ	time phase shift between the chambers

REFERENCES

1. Fung YC, Yih CS. Peristaltic transport. *Journal of Applied Mechanics ASME* 1968; **35**: 669–675.
2. Shapiro AH, Jaffrin MY, Weinberg SL. Peristaltic pumping with long wavelengths at low Reynolds number. *Journal of Fluid Mechanics* 1969; **37**: 799–825.
3. Provost AM, Schwarz WH. A theoretical study of viscous effects in peristaltic pumping. *Journal of Fluid Mechanics* 1994; **279**: 177–195.
4. Li M, Brasseur JG. Non-steady transport in finite-length tubes. *Journal of Fluid Mechanics* 1993; **248**: 129–151.
5. Blackshear PL, Blackshear GL. *Mechanical Hemolysis*. McGraw-Hill: New York, 1987.
6. Bludszuweit C. Model for a general mechanical blood damage prediction. *Artificial Organs* 1995; **19**: 583–589.
7. Tu C, Deville M, Dheur L, Vanderschuren L. Finite element simulation of pulsatile flow through arterial stenosis. *Journal of Biomechanics* 1992; **25**: 1141–1152.
8. Bluestein D, Niu L, Schoephoerster RT, Dewanjee MK. Fluid mechanics of arterial stenosis: relationship of the development of mural thrombus. *Annals of Biomedical Engineering* 1997; **25**: 344–356.

9. Fluent. *FIDAP*. Fluent Incorporated: Centerra Resource Park, Lebanon, NH 03766-1442, U.S.A., 1998.
10. Uchida S, Aoki H. Unsteady flows in a semi-infinite contracting or expanding pipe. *Journal of Fluid Mechanics* 1977; **82**: 371–387.
11. Robertson JM, Clark ME, Cheng LC. A study of the effect of a transversely moving boundary on plane Poiseuille flow. *Journal of Biomechanical Engineering ASME* 1982; **104**: 314–323.
12. Ramstack JM, Zuckerman L, Mockros LF. Shear-induced activation of platelets. *Journal of Biomechanics* 1979; **12**: 113–125.

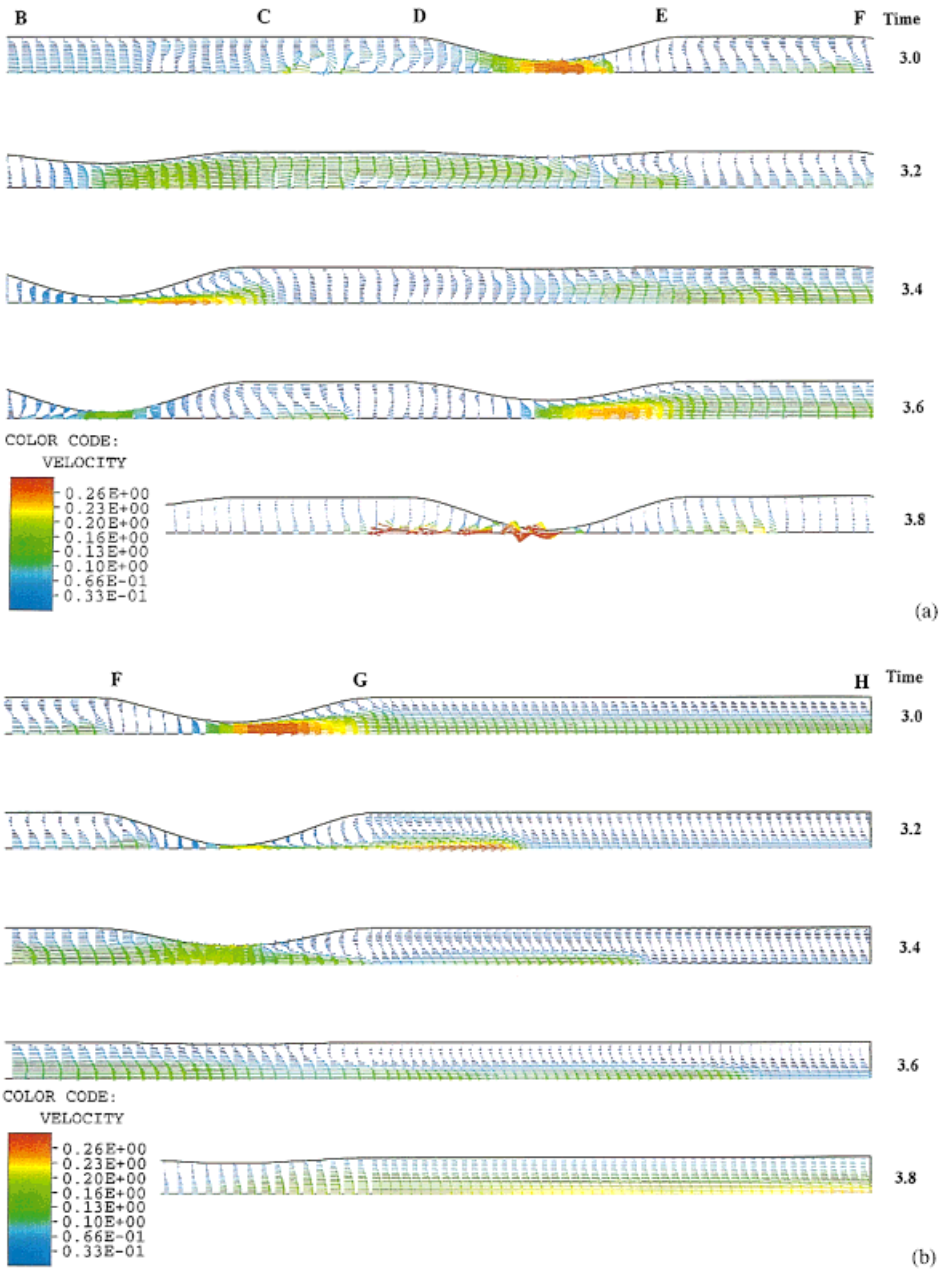

Plate 1. (a) Inlet velocity field from $t = 3.0$ at 0.2 s intervals; (b) outlet velocity field from $t = 3.0$ at 0.2 s intervals.

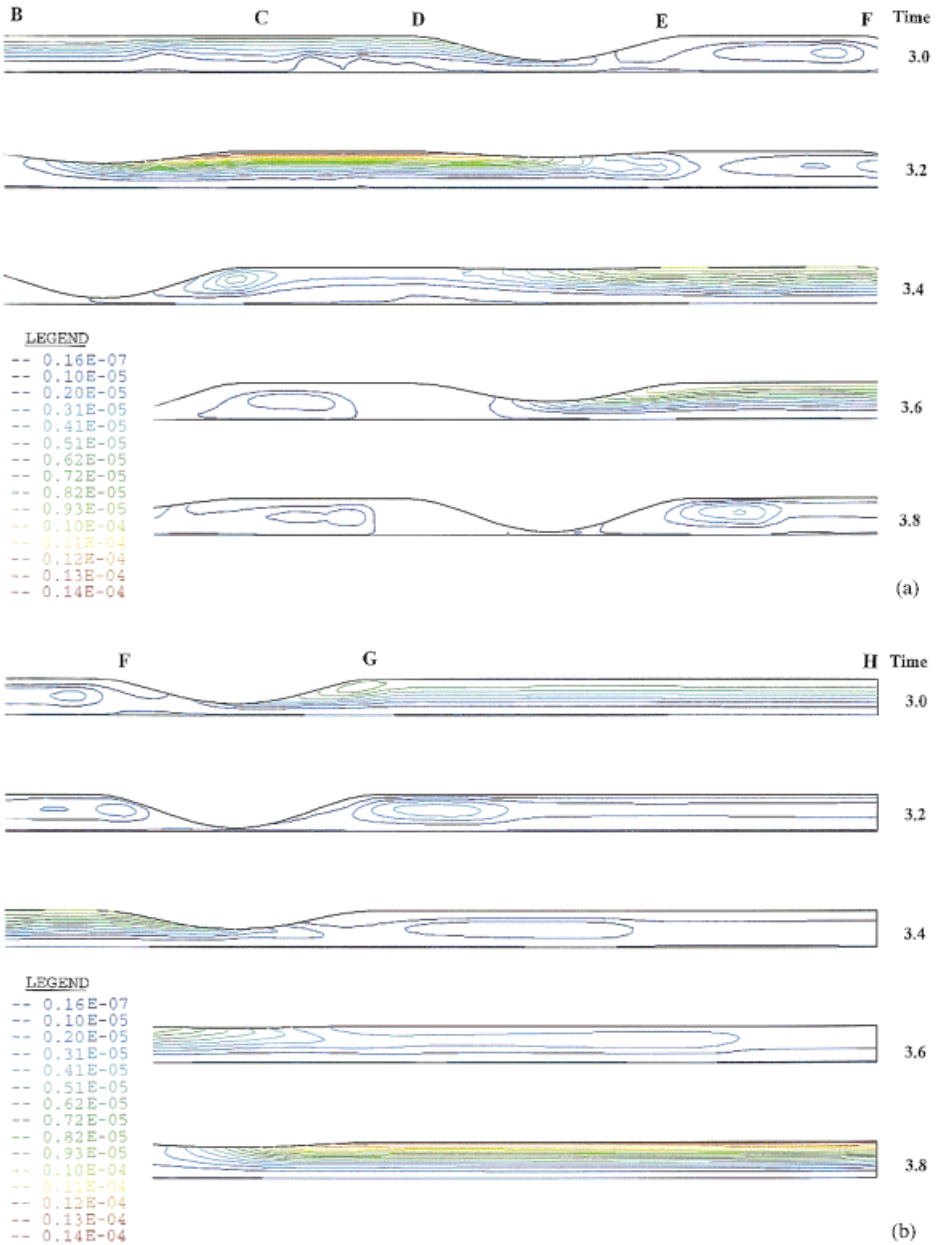

Plate 2. (a) Inlet streamline contour plot form $t = 3.0$ at 0.2 s intervals; (b) outlet streamline contour plot from $t = 3.0$ at 0.2 s intervals.